









3D printing of structural gradient soft actuators by variation of bioinspired architectures

Luquan Ren¹ , Bingqian Li¹ , Zhengyi Song¹ , Qingping Liu^{1,*} , Lei Ren^{1,2,*} , and Xueli Zhou¹ 

¹Key Laboratory of Bionic Engineering (Ministry of Education), Jilin University, Changchun 130022, China

²School of Mechanical, Aerospace and Civil Engineering, University of Manchester, Manchester M13 9PL, UK

Received: 2 November 2018

Accepted: 9 January 2019

Published online:
17 January 2019

© Springer Science+Business Media, LLC, part of Springer Nature 2019

ABSTRACT

Soft actuators, which ensure the safety of robot–human interactions, extend the range of robotic operations to fragile and sensitive objects. Shape memory polymers are one of the building material for soft actuators due to their spontaneous shape memory properties under stimulation. However, the global, discontinuous and imprecise motion put significant limitations on their wide application. Recently, it has been demonstrated that by using motifs in nature, anisotropic, heterogeneous properties of soft actuators can be fabricated. Here, it is shown that soft actuators with local response and continuously varying shape memory properties can be realized through integrating bioinspired arranged building blocks (fibers). The modified 3D printing technique provides the pathway of assembling these fibers as designed. We have revealed the underlying mechanism of the formation of gradient shape memory properties. Simulations successfully demonstrate the feasibility of our approach to manipulate shape memory behaviors. The translation of nature’s design motifs offers synthetic soft actuators the opportunity towards unprecedented applications such as soft robot, drug carrier and other intelligent applications.

Introduction

Gradient is a widespread strategy in nature for the purpose of survival and reproduction [1]. The introduction of spatial gradients can effectively enhance the mechanical and dynamic performance of materials by, for example, alleviating stress concentrations and creating anisotropic hygroscopicity [2–5]. Gradient is used to referring to gradient chemical

compositions/constituents without clear boundaries [6]. The term employed here in its broad sense is to describe the site-specific properties distributed within a material with gradual transitions between dissimilar nano-/micro-structural features, which is to say, structural gradient.

Structural gradient is a common approach utilized by biological materials to realize self-morphing and self-adaption. More specifically, it is fundamentally associated with the variations in structural

Address correspondence to E-mail: liuqp@jlu.edu.cn; lei.ren@manchester.ac.uk

characteristics containing arrangements [7, 8], distributions [9, 10], dimensions [11, 12], and orientations [13, 14] of the building units. Among all these characteristics, the most widespread tool to achieve structural gradient is employing anisotropic building units, such as fibers, lamellae, platelets and tubules, with properties that strongly depend on orientation [15, 16]. By orienting these fillers, nature has created many fascinating artworks.

There are basically two approaches to realize “orientation gradient”. One way is arranging these building blocks from disordered to ordered. A typical example is the biopolymer-based wheat awn [7, 17]. In order to drive the seed into soil for dispersal, wheat awn has evolved into the structure that the cellulose fibrils are very well aligned along the long axis in the cap yet randomly organized at the ridge. The asymmetry in this arrangement leads to non-uniform expansion between different regions when exposed to daily humidity cycles, thereby providing the driving force for its dispersal.

The other way is tuning the orientations of these building units to achieve gradual transition. To adapt to the environment and their own weight, many tissues in nature have adopted this strategy. In softwood branches, the alignment of fibrils changes from the lower side near the trunk, where the fibrils show a large deviation with respect to the long axis (with the microfibril angle of 40°), to the upper side of the branch where the fibrils are almost parallel to the long axis [10, 18]. This helps the bending of the branch upwards to accommodate its own weight.

Although nature has developed such abundant prototypes for us to learn, few has been synthesized so far due to limited capacity of current manufacturing technology. Recently, the emergence of 3D printing (top-down method), which resembles the way of growth of biological tissues, offers the avenue of fabricating soft actuators with precisely built constituents and architectures [19–21].

Recently, there are many soft actuators that rely on regulating fiber orientations to implement anisotropic response [22–24]. Shape memory polymers are smart material with the ability to return from a deformed state to their original state when heated above glass transition temperature (t_g). Due to the low strength and long response time, numerous efforts have been devoted to endow SMPs with global reinforced properties containing reduced recovery time and increased modulus [25, 26]. However, these methods

are unable to realize soft actuators with localized and gradient properties, which is the capacity soft actuator requires [27].

In this work, we have fabricated gradient soft actuators mimicking the “structural gradient” design in biological materials via modified magnetically assisted stereolithography 3d printing. To mimic the structures of wheat awn and softwood branches, the intensity and the walking path of the magnetic field are manipulated to regulate gradient changes of the degree of orientation and oriented angles, respectively. We have established the structure–property relationships and uncovered the underlying governing mechanisms. This method opens the new pathway towards manufacturing more flexible and locally controllable soft actuators.

Experiment

Materials

The photosensitive resins are mixture of clear resin (Clear FLGPCL04, Formlabs corp., US) and flexible resin (Flexible FLFLGR02, Formlabs corp., US) in a ratio of 3:2. The sieved short steel fibers (SSFs) with an average aspect ratio of 168 (analysis of C, Si, Mn, S, P, Dezhou Fangyuan Steel Wool Fiber Co., Ltd, China) were added into the matrix in the mass/volume ratio 2:5. Fumed silica with 0.1 wt% was introduced to prevent the fibers from settling. These constituents were homogenized with a mechanical stirrer (FSH-2A, China) for 20 min. All reagents were directly used without any purifications or modifications.

3D printing of shape memory stripes with gradiently aligned fibers

A modified magnetically assisted stereolithography 3d printer (Fig. 1a) was developed to print composites with aligned SSFs. Two pistons named as feed piston and build piston were used to fill the resin-fiber slurry and print the parts respectively. As shown in Fig. 1b, the printer first spreads a layer of slurry on the building piston by the moving blade. Subsequently, the permanent magnet moves from right to left side of the building unit with constantly changing walking path and height, causing the fibers in the slurry aligned in varying angles and in varying

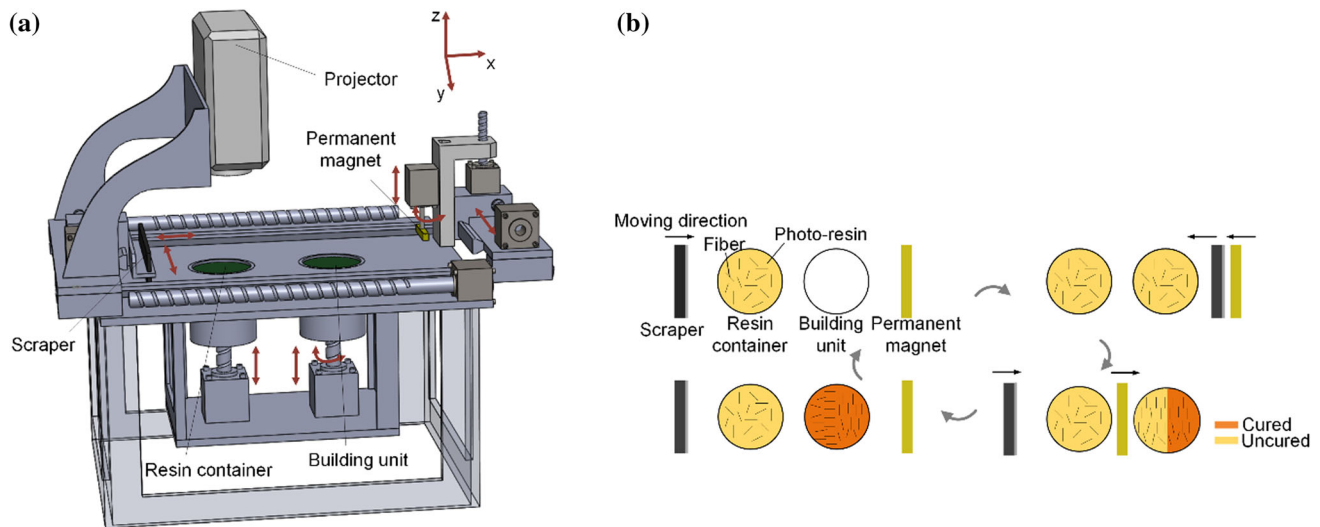


Figure 1 3D printing of shape memory stripes with aligned fibers. **a** The magnetically assisted slurry-based stereolithography 3D printer. **b** Diagram of the 3D printing process.

degrees of orientation. A mask-image-projection is used to cure part of the slurry. When the permanent magnet moves from left to right side of the building unit, it rotates a specific angle around z axis or tunes its height along z axis at the same time, enabling the remaining part of the slurry aligned. It is worth mentioning that the moving direction is always perpendicular to long axis of the permanent magnetic stripe. If there are more divided areas, more cycles will be required until all areas are cured. Then the feed piston comes up and the build piston drops one layer. The building unit could rotate around z axis if needed (Fig. 1b). After that the printer spreads a new layer of slurry and repeats the process above until the entire part is printed. Each sample with the same angle shall have 2 copies.

Material characterization and folding measurement

Image J software supported by an oval profile plug-in was utilized to characterize the degree of alignment of fibers. Two Dimensional (2D) Fast Fourier Transform (FFT) analysis was conducted, and the FFT Frequency image with long stripes radiating from the center point represents the high frequency of the fibers arranged at the angle. In the normalized intensity values plot, the peak shape and height determine the degree of alignment, and the peak position indicates the principle axis of orientation of the fibers.

Dynamic mechanical analysis (DMA) test was conducted to investigate the glass transition temperature and storage modulus in different temperatures. It was performed with a dynamic mechanical analyzer (Model Q800, TA Instruments, New Castle, DE, USA) in the uniaxial tension mode. A preload of 1 mN was applied on the sample (40 mm × 5 mm × 0.8 mm) and the strain was oscillated at a frequency of 1 Hz with the peak-to-peak amplitude of 0.1%.

The bending profiles were captured by a digital camera and the corresponding bending angles were measured by Digimizer software. A magnetometer (HT20, HT, China) was used to analyze the magnetic intensity of the permanent stripe.

Results and discussion

Preparation of the bioinspired structural gradient stripes

In our experiment, two sorts of commercial available photo-resins, namely clear resin and flexible resin, were mixed in a mass ratio 3: 2 to enable the blends with both preferable strength and shape memory characteristics based on our previous researches. The sieved short steel fibers (SSFs) were added into above matrix in the mass/volume ratio 2:5 and homogenized with a mechanical stirrer [28]. To investigate thermomechanical performance of our samples, dynamic mechanical analysis (DMA) test was

conducted and the glass transition temperature (T_g) was 60 °C, corresponding to the peak of the Tan Delta curve in Fig. 8b.

A modified magnetically assisted stereolithography 3d printer (Fig. 1a) was developed to fabricate composites with gradient aligned SSFs. Specific manufacturing process is introduced in Experiment section (Fig. 1b). Two sorts of gradients containing gradual transition of degrees of orientation and oriented angles have been fabricated. In the first case, varying degree of orientations are conferred by the moving freedom along the z axis of the magnetic strip. The lower the magnetic strip, the greater the magnetic field intensity. Within a certain magnetic intensity range, as the intensity increases, the degree of orientation turns larger. A stepper motor was used to tuning the magnetic strip along z axis continuously during its moving along the x axis. The second sort of gradient is implemented by the rotation of the magnetic strip around the z axis, which is manipulated by another independent motor. Therefore, this motion can also be superimposed with other mode of motions. By controlling the height and walking path of the magnetic strip, the structures with fibers gradiently converting from disordered to ordered, and from one angle to another could be fabricated.

To mimic this design of wheat awn (gradual transition of degrees of orientation), we programmed the height of the magnetic strip during its walking along x axis to achieve gradual transition from disorder to order as shown in Fig. 2a, b. To fabricate the structures of softwood branches (gradual transition of oriented angles), we manipulated the rotation of the magnetic strip around the z axis to fabricated stripes with fibers gradually transited from one angle to another (Fig. 2c, d) [29–31].

Regulation and characterization of the degree of orientation of fibers

A crucial step for understanding the aligning rules is to figure out the relationship between the height and intensity of the magnetic stripe. A magnetometer was used to analyze the field intensity at varying heights of the permanent stripe. In Fig. 3a, as the height of the permanent magnet increases from 1 to 25 mm, the intensity of the magnetic field gradually decreases from 190 to 5 mT.

Image J software supported by an oval profile plug-in was utilized to characterize the degree of

alignment of fibers [32, 33]. Detailed characterization process is shown in Fig. S1. Basically, there are three regions for the degree of orientation S with the rising of the field intensity (Fig. 3b). When the intensity is smaller than 5 mT, the fibers in the slurry can not be effectively aligned due to the viscosity of the matrix (this invalid region has not been recorded). When the intensity lies between 5 and 15 mT, the orientation degree is positively related to the intensity. Once surpassing the upper threshold, the orientation degree decreases with the rising of the intensity. This is possibly due to that the excessive intensity will cause the fibers to follow the travelling path of the magnetic stripe in the matrix, resulting in accumulating or even completely adsorbed on the magnetic strip.

The influence of intensity and walking path of the magnetic field on shape memory properties

We printed 5 stripes with fibers arranged under the intensity of the magnetic field of 5, 8, 14, 26, 70 mT, corresponding to the height of the magnetic stripe of 2.5, 2, 1.5, 1, 0.5 mm. During their shape recovery, we noticed the stripes printed under different magnetic field intensity generated various recovered curvatures. In Fig. 4a, we observed that there is a valley of the recovered curvature where the stripe has the maximum shape recovery ratio. Before the valley, the curvatures are decreasing with the rising of the field intensity. After this threshold, the curvatures are increasing as field intensity rises. We discovered that the threshold of the recovered curvatures is also that of the degree of orientation. Before this point, the rising field intensity will lead to better aligned fibers, after which the degree of orientation will decrease due to accumulating or adsorption caused by excess amount of field intensity.

The other factor we should focus on is the influence of the oriented angles. We have arranged the angles θ as 0°, 15°, 30°, 45°, 60°, 75°, 90° by rotating the permanent stripe (maintaining the height at 2 mm). In Fig. 4b, the recovered curvatures are increasing with the angles, which indicates the shape recovery ratio is positively related to the oriented angles. The inset is used to illustrate the definition of the angle θ .

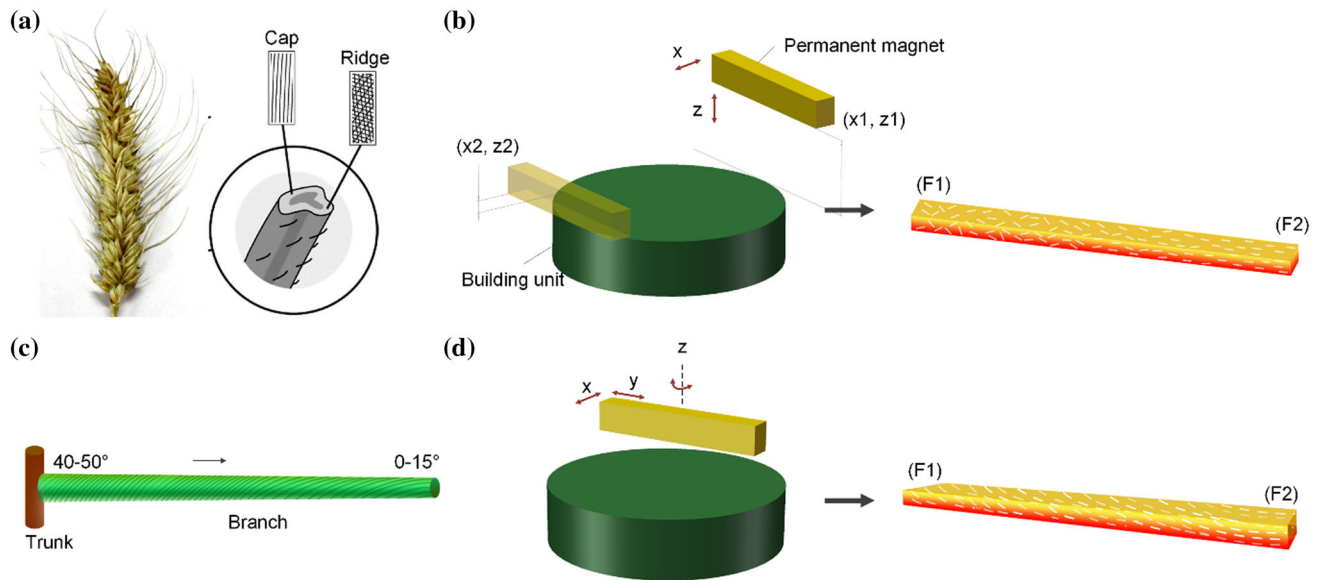


Figure 2 The structural gradient of biological materials and the methods exploited to mimic their structures. **a** The microstructure of the wheat awn. **b** The schematic of the method of fabricating composites with fibers arranged from disordered to ordered. **c** The

microstructure of softwood branches. **d** The schematic of the method used for fabricating composites with fibers aligned from one angle to another.

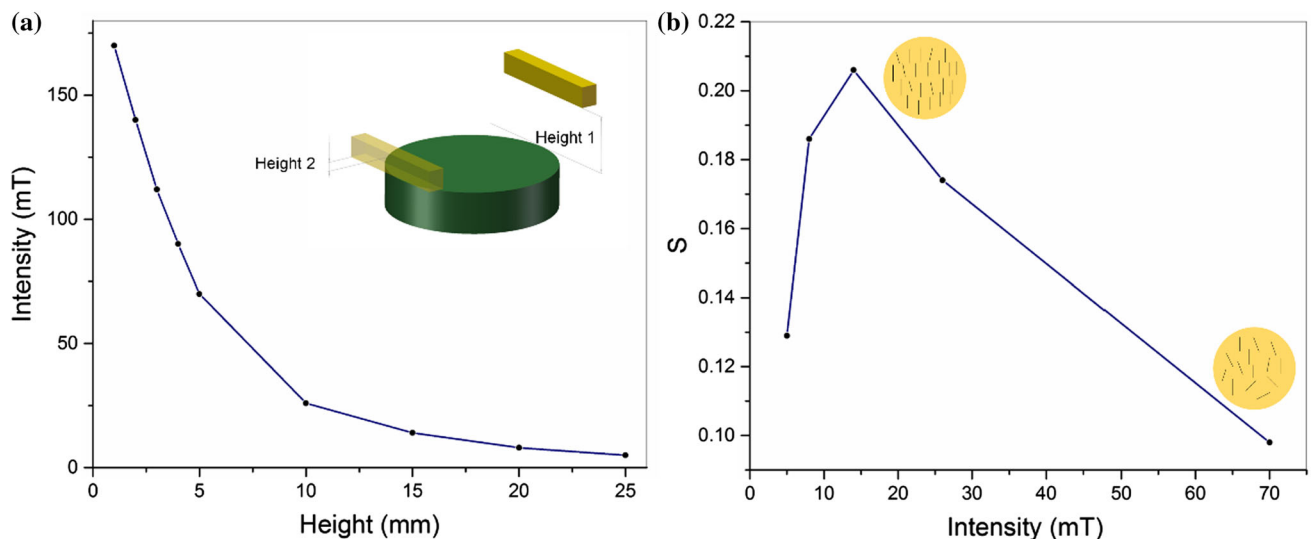


Figure 3 The varying degrees of orientation with rising heights of the permanent magnetic stripes. **a** The changing trend of field intensity with increasing height of the permanent stripe. **b** The changing trend of degree of orientation with the rising intensity of the magnetic field.

The shape memory process of structural gradient composites

The shape memory process was conducted following these three steps. Firstly, the sample was heated to 60 °C and put into an arched mold. Then, the mold with sample was cooled to 20 °C to freeze the temporary shape. Finally, the sample was taken out of the mold and reheated to 60 °C to recover the

permanent shape [34]. Specific shape memory process is illustrated in Fig. 5.

In this part, we printed stripes with gradient arranged structures and analyzed their gradient varying shape memory properties. Although printed with the same composition, their microstructures impart them different properties. Both methods mentioned above have been implemented to produce gradient microstructure.

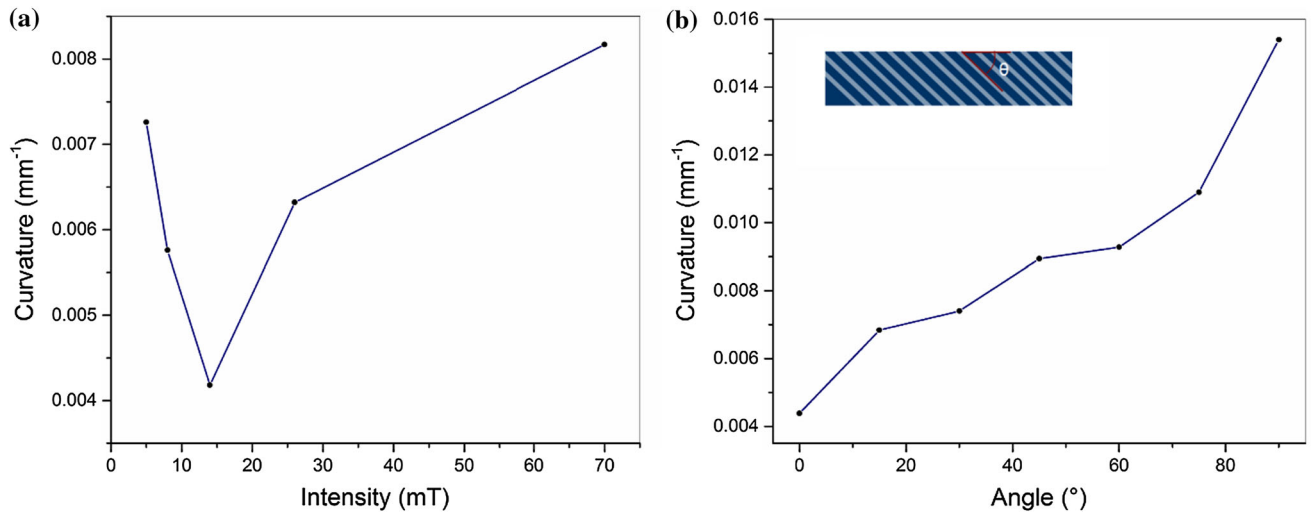
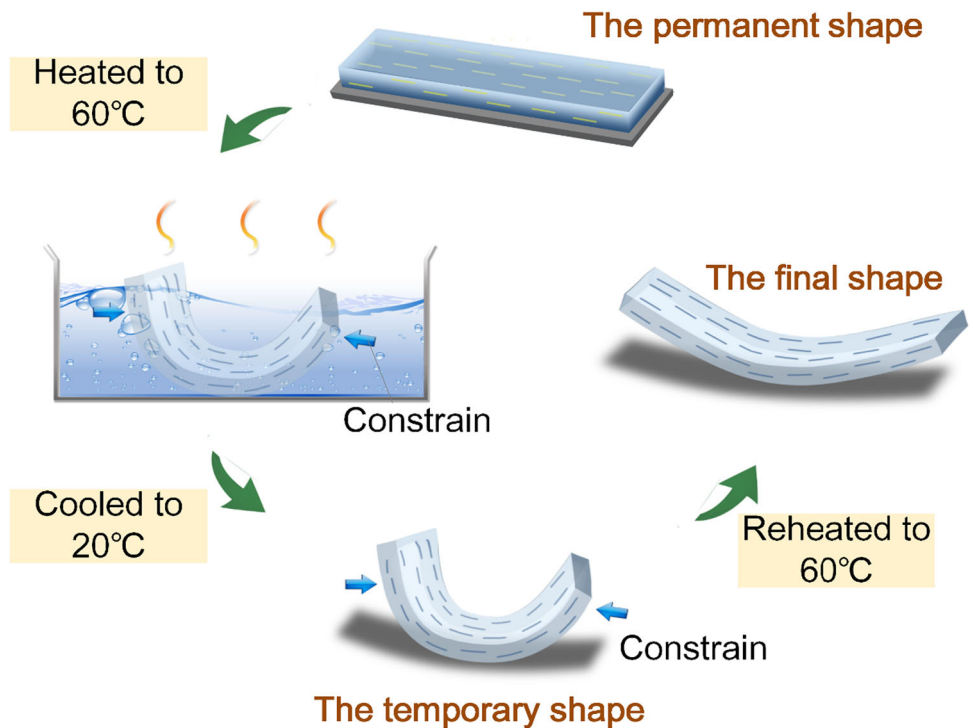


Figure 4 The different curvatures corresponding to increasing field intensity and arranged angles. **a** The curvatures of recovered shapes printed at various field intensity. **b** The curvatures of recovered shapes printed with increasing angles.

Figure 5 Schematic of the shape memory process. The strip was fabricated to be flat. Afterwards it was programmed in 60 °C hot water with an arched mold obtained by 3D printing. While the constrain was applied, it was cooled to 20 °C to fix the temporary shape. When reheated to 60 °C, it would recover the permanent shape.



First, we exploited the method of adjusting the height to achieve gradient degree of orientation. 3D printed circular mold was used to program the temporary shapes (Fig. 6a). The purpose of circular mold is to ensure that each local region of the temporary shape owns the same initial curvature, which provides the condition to reflect the differences in shape recovery process. Subsequently, we placed the programmed stripes into hot water at 60 °C for shape

recovery. It was shown that different local regions of the stripes possess different recovery ratea (Fig. 6b), which resulted in a faster recovered speed of the left side (with fibers arranged along the long axis) compared to the right side (with fibers randomly arranged). When the recovery process accomplished at 50 s, the curvature of left side was smaller than that of right side, which indicated a higher shape recovery

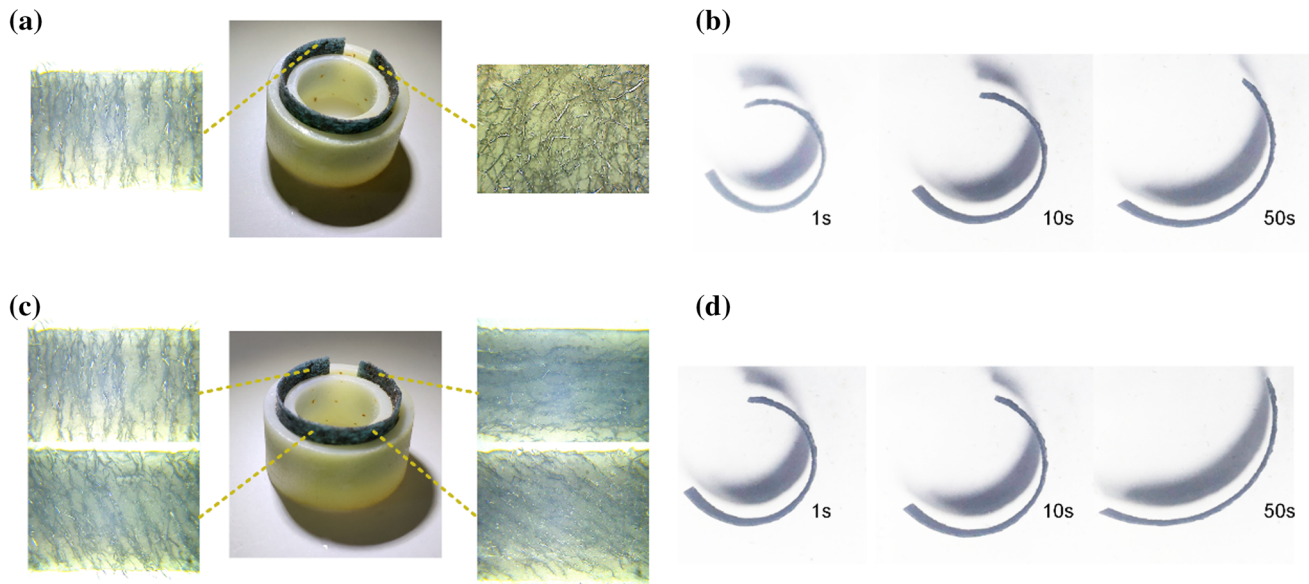


Figure 6 The shape recovery process of gradient arranged stripes. **a** Programming of stripes with gradient degrees of orientation. **b** The shape recovery process of stripes with gradient degrees of

orientation. **c** Programming of stripes with gradient oriented angles. **d** The shape recovery process of stripes with gradient oriented angles.

ratio of the region with fibers arranged along the long axis.

Similarly, by adjusting the path travelled by the magnetic strip, the angles of the fibers can be arranged gradiently (from 0° (left) to 90° (right)) (Fig. 6c). By imparting circular temporary shape, we observed that the above phenomenon that the recovery rate of left side is larger than the right side occurs again. Meanwhile, the left side has a higher shape recovery ratio (Fig. 6d). However, the differences lie in shape recovery ratio that the side aligned in 90° is smaller than the side with random arrangement, nevertheless, larger in recovery rate. Overall, the stripes with fiber arranged from 0° to 90° have a more thorough recovery. Specific reason will be parsed in subsequent section.

Investigation of the influencing parameters on per unit variation of shape memory properties

In fact, if the height of the magnetic strip is proportionally decreased (with the acceleration of a_h) or its angle is proportionally changed (with the acceleration of a_θ), the recovered curvature will vary accordingly with the acceleration of a_c , which has a significant impact on deformation behaviors. We named the per unit variation of shape memory

properties caused by the variation of the degree of orientation and the variation of angles as Δp . We set Δp of each two adjacent units as 1, 2, 4. Due to large size of our fibers and relatively smaller area of the 3D printing building platform, it is difficult to analyze the effect of Δp through experiment. Therefore, simulation was conducted to qualitatively analyze its impact. In simulation, Δp is reflected by the changes of expansion ratio (Abaqus CAE). These changes in expansion rate are essentially the change of microstructures attributed to the acceleration of the height change (a_h) and the acceleration of the angle change (a_θ) of the magnetic stripe. We have not yet fully understood the quantitative effect of changes in degree of orientation or angle on shape memory properties, and no mathematical model has been established. This is the further work to be done.

As the Δp increases from 1, 2 to 4, its recovered shape transforms from a circle to an involute curve (Fig. 7a, b, c), and the curvature from left to right side become more distinct. Similarly, gradient varying curvatures in symmetrical forms will also be feasible (Fig. 7d, e, f) by setting Δp as ± 1 , ± 2 , ± 4 . It is worth noting that the height and angular velocity cannot exceed the corresponding ranges. Too small height will cause the fibers to aggregate or adsorb on the magnetic strip. However, exceedingly large height will result in insufficient magnetic field strength to

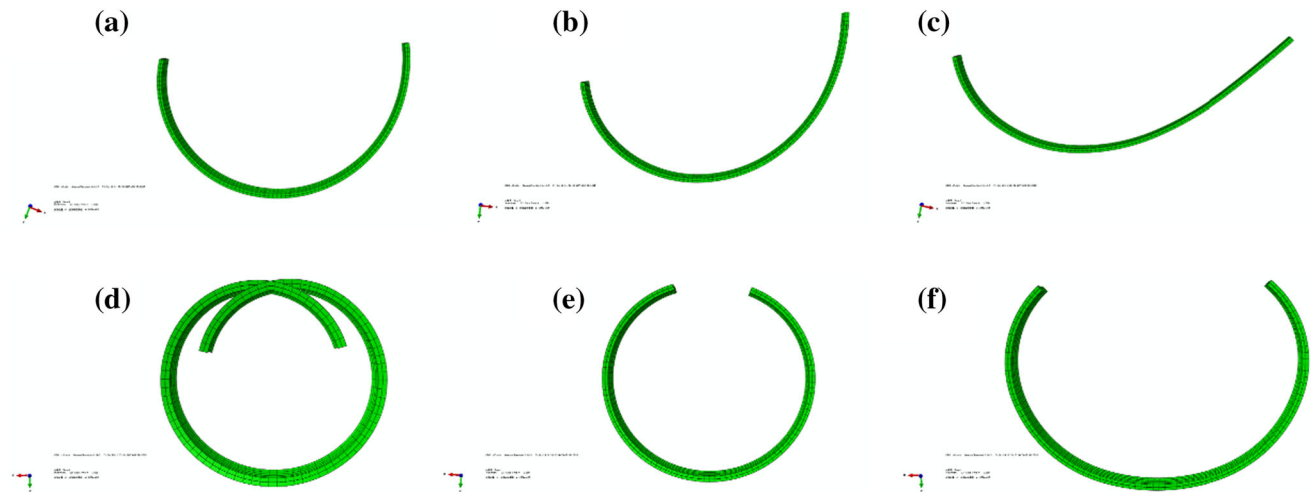


Figure 7 Simulations to qualitative analyze the impact of acceleration. **a** The curve with the value of acceleration (Δp) of 1. **b** The curve with the value of acceleration (Δp) of 2. **c** The curve with the value of acceleration (Δp) of 4. **d** The curve with

the value of acceleration (Δp) of ± 1 in symmetrical form. **e** The curve with the value of acceleration (Δp) of ± 2 in symmetrical form. **f** The curve with the value of acceleration of ± 4 in symmetrical form.

exert a torque on the fibers. Furthermore, excessive angular velocity will make the magnetic field not have enough time to orient the fibers.

The underlying controlling mechanism of shape recovery properties

To study the relationship between shape recovery properties and fiber arrangements, the hyperelasticity theory proposed by deBotton and other researchers was utilized [34–36] and it was expressed as

$$\delta = -p\mathbf{I} + \underbrace{\mu_a \mathbf{F}(\mathbf{F})^T}_{\text{iso}} + \underbrace{\mu_b (1 - I_4^{-\frac{3}{2}}) \mathbf{F}a_0 \otimes \mathbf{F}a_0}_{\text{aniso}} \quad (1)$$

$$\mu_a = \frac{(1 - v_f)\mu_m + (1 + v_f)\mu_f}{(1 + v_f)\mu_m + (1 - v_f)\mu_f} \quad (2)$$

$$\mu_b = \frac{(\mu_f - \mu_m)^2 v_m v_f}{(1 + v_f)\mu_m + (1 - v_f)\mu_f} \quad (3)$$

$$I_4 = a_0(Ca_0) \quad (4)$$

where μ_m and μ_f are shear moduli of the matrix and the fibers, respectively; v_m and v_f are volume fraction of the matrix and the fibers. \mathbf{I} refers to its principle invariant and C is the right Cauchy–Green deformation tensor. I_4 is the deformation that changes along the length of the fibers and a_0 is the fiber direction in the reference configuration. In Eq. [1], p is an

arbitrary hydrostatic pressure, the second term is associated with the isotropic part of the Cauchy stress and the third term is associated with anisotropic part of the Cauchy stress.

Based on the above equations, the Cauchy stress of composite is positively related to the degree of anisotropic and shear moduli of the matrix and the fibers. The DMA test in Fig. 8a has shown that smaller angles (comparing 0° to 45° and 90°) will lead to greater modulus, and greater modulus of the matrix and the fibers will contribute to larger Cauchy stress. Therefore, the stripes with smaller angle and higher degrees of orientation have larger recovery force and thus larger recovery ratio. In addition, we observed that as the temperature increases, the storage modulus of the material decreases. So we heat the stripes to 60°C to enable the material to possess as large recovery force as possible.

Conclusion

In this work, we have printed bioinspired gradient structural materials mimicking the deformation behaviors in nature. The tunable intensity of the magnetic field and variable walking path have been exploited to determine gradient changes of degrees of orientation and oriented angles, respectively. Higher intensity in certain range and smaller angle will promote higher shape recovery ratio. Moreover, we

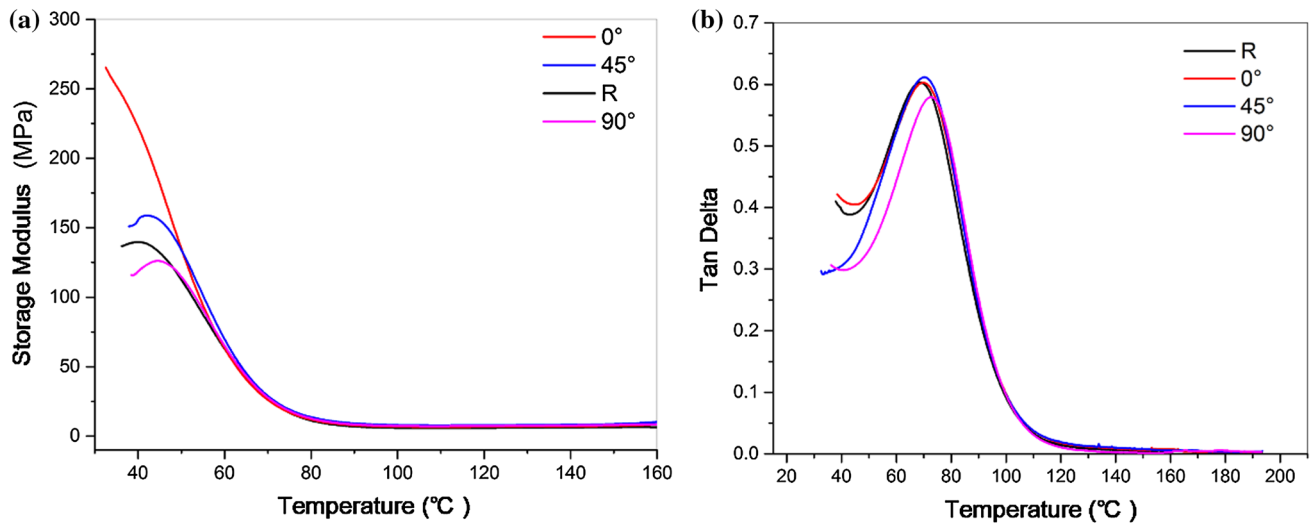


Figure 8 The results of DMA test for differently arranged stripes. **a** Storage modulus of orderly arranged and randomly distributed stripes (40 mm × 5 mm × 0.8 mm). Fibers are oriented at the

angle of 0°, 45° and 90° to x axis (the loading direction). **b** Tan Delta of orderly arranged and randomly distributed stripes.

have simulated the structures with varying changing rates of shape memory properties (with acceleration of Δp), which is regulated by controlling the acceleration of the height change (a_h) and the acceleration of the angle change (a_θ) of the magnetic stripe. The underlying mechanism of the formation of gradient shape memory properties has been revealed. However, mathematical model about changes in degree of orientation or angle on shape memory properties has not been established, which needs further effort to be accomplished. The bioinspired structural gradient shape memory composites introduced here have the potential to fabricate soft actuators with gradient and continuous locomotion, which can offer assistance to soft robots, drug carriers, satellites and other intelligent applications.

Acknowledgements

This research was supported by National Key R&D Program of China (2018YFB1105100) and the Key Scientific and Technological Project of Jilin Province (No. 20170204061GX).

Electronic supplementary material: The online version of this article (<https://doi.org/10.1007/s10853-019-03344-8>) contains supplementary material, which is available to authorized users.

References

- [1] Liu Z, Meyers MA, Zhang Z, Ritchie RO (2017) Functional gradients and heterogeneities in biological materials: design principles, functions, and bioinspired applications. *Prog Mater Sci* 88:467–498
- [2] Studart AR (2013) Biological and bioinspired composites with spatially tunable heterogeneous architectures. *Adv Funct Mater* 23:4423–4436
- [3] Murphy T (2010) Gradients of dentine exposure in human molar tooth attrition. *Am J Phys Anthropol* 17:179–186
- [4] Miserez A, Schneberk T, Sun C, Zok FW, Waite JH (2008) The transition from stiff to compliant materials in squid beaks. *Science* 319:1816–1819
- [5] Chen Y, Wang L, Xue Y, Jiang L, Zheng Y (2013) Bioinspired tilt-angle fabricated structure gradient fibers: micro-drops fast transport in a long-distance. *Sci Rep* 3:2927
- [6] Bentov S, Zaslansky P, Alsawalmih A, Masic A, Fratzl P, Sagi A et al (2012) Enamel-like apatite crown covering amorphous mineral in a crayfish mandible. *Nat Commun* 3:839
- [7] Elbaum R, Zaltzman L, Burgert I, Fratzl P (2007) The role of wheat awns in the seed dispersal unit. *Science* 316:884–886
- [8] Dawson C, Vincent JFV, Rocca AM (1997) How pine cones open. *Nature* 390:668
- [9] Gibson LJ (2012) The hierarchical structure and mechanics of plant materials. *J R Soc Interface* 9:2749–2766
- [10] Eder M, Jungnickl K, Burgert I (2009) A close-up view of wood structure and properties across a growth ring of norway spruce. *Trees* 23:79–84

- [11] Tadayan M, Amini S, Masic A, Miserez A (2015) Saddle structures: the mantis shrimp saddle: a biological spring combining stiffness and flexibility. *Adv Funct Mater* 25:6429
- [12] Miserez A, Weaver JC, Thurner PJ, Aizenberg J, Dauphin Y, Fratzl P, Morse DE, Zok FW (2008) Effects of laminate architecture on fracture resistance of sponge biosilica: lessons from nature. *Adv Funct Mater* 18:1241–1248
- [13] Färber J, Lichtenegger HC, Reiterer A, Stanzl-Tschegg S, Fratzl P (2001) Cellulose microfibril angles in a spruce branch and mechanical implications. *J Mater Sci* 36:5087–5092. <https://doi.org/10.1023/A:1012465005607>
- [14] Zhang Y, Paris O, Terrill NJ, Gupta HS (2016) Uncovering three-dimensional gradients in fibrillar orientation in an impact-resistant biological armour. *Sci Rep* 6:26249
- [15] Raabe D, Sachs C, Romano P (2005) The crustacean exoskeleton as an example of a structurally and mechanically graded biological nanocomposite material. *Acta Mater* 53:4281–4292
- [16] Watanabe T, Imamura Y, Hosaka Y, Ueda H, Takehana K (2007) Graded arrangement of collagen fibrils in the equine superficial digital flexor tendon. *Connect Tissue Res* 48:332–337
- [17] Elbaum R, Gorb S, Fratzl P (2008) Structures in the cell wall that enable hygroscopic movement of wheat awns. *J Struct Biol* 164:101–107
- [18] Studart AR, Erb RM (2014) Bioinspired materials that self-shape through programmed microstructures. *Soft Matter* 10:1284–1294
- [19] Yang Y, Chen Z, Song X, Zhang Z, Zhang J, Shung KK, Zhou Q, Chen Y (2017) Biomimetic anisotropic reinforcement architectures by electrically assisted nanocomposite 3d printing. *Adv Mater* 29:1605750
- [20] Collino RR, Ray TR, Fleming RC, Sasaki CH, Haj-Hariri H, Begley MR (2015) Acoustic field controlled patterning and assembly of anisotropic particles. *EML* 5:37–46
- [21] Martin JJ, Fiore BE, Erb RM (2015) Designing bioinspired composite reinforcement architectures via 3d magnetic printing. *Nat Commun* 6:8641
- [22] Rudykh S, Boyce MC (2014) Transforming small localized loading into large rotational motion in soft anisotropically structured materials. *Adv Eng Mater* 16:1311–1317
- [23] Slesarenko V, Engelkemier S, Galich PI, Vladimirovsky D, Klein G, Rudykh S (2018) Strategies to control performance of 3d-printed, cable-driven soft polymer actuators: from simple architectures to gripper prototype. *Polymers* 10:846
- [24] Galich PI, Slesarenko V, Rudykh S (2016) Shear wave propagation in finitely deformed 3D fiber-reinforced composites. *Int J Solids Struct* 110–111:294–304
- [25] Bin S, Kim JG, Nam YY, Lee GH, Yu WR (2015) Mechanical analysis of carbon fiber shape memory polymer composites. In: *World congress on advances in structural engineering and mechanics*
- [26] Ge Q, Luo X, Rodriguez ED, Zhang X, Mather PT, Dunn ML, Qi HJ (2012) Thermomechanical behavior of shape memory elastomeric composites. *J Mech Phys Solids* 60:67–83
- [27] Kumar S, Reddy KVVS, Kumar A, Devi GR (2013) Development and characterization of polymer–ceramic continuous fiber reinforced functionally graded composites for aerospace application. *Trends Cardiovasc Med* 26:185–191
- [28] Illeperuma WRK, Sun JY, Suo Z, Vlassak JJ (2014) Fiber-reinforced tough hydrogels. *EML* 1:90–96
- [29] Erb RM, Sander JS, Grisch R, Studart AR (2013) Self-shaping composites with programmable bioinspired microstructures. *Nat Commun* 4:1712
- [30] Wegst UG, Bai H, Saiz E, Tomsia AP, Ritchie RO (2015) Bioinspired structural materials. *Nat Mater* 14:23–36
- [31] Naleway SE, Porter MM, Mckittrick J, Meyers MA (2015) Structural design elements in biological materials: application to bioinspiration. *Adv Mater* 27:5455–5476
- [32] Mahajan C, Cormier D (2015) 3D printing of carbon fiber composites with preferentially aligned fibers. In: *IIE annual conference. Proceedings*
- [33] Ayres C, Bowlin GL, Henderson SC, Taylor L, Shultz J, Alexander J, Telemeco TA, Simpson DG (2006) Modulation of anisotropy in electrospun tissue-engineering scaffolds: analysis of fiber alignment by the fast fourier transform. *Biomaterials* 27:5524–5534
- [34] Ge Q, Serjouei A, Qi HJ, Dunn ML (2016) Thermomechanics of printed anisotropic shape memory elastomeric composites. *Int J Solids Struct* 102–103:186–199
- [35] Debotton G, Hariton I, Socolsky EA (2016) Neo-Hookean fiber-reinforced composites in finite elasticity. *J Mech Phys Solids* 54:533–559
- [36] Idiart MI (2016) Modeling the macroscopic behavior of two-phase nonlinear composites by infinite-rank laminates. *J Mech Phys Solids* 56:2599–2617